Research Square

Preprints are preliminary reports that have not undergone peer review.
They should not be considered conclusive, used to inform clinical practice,
or referenced by the media as validated information.

Cascading Impacts of AMOC weakening and collapse on Marine Biogeochemistry

Paul Lerner

pel2119@columbia.edu

Columbia Univeresity/NASA Goddard Institute for Space Studies/Columbia University
https://orcid.org/0000-0003-4751-0262

Anastasia Romanou

Columbia University

Article

Keywords:

Posted Date: May 8th, 2026

DOI: https://doi.org/10.21203/rs.3.rs-9044876/v1

License: This work is licensed under a Creative Commons Attribution 4.0 International License.
Read Full License

Additional Declarations: There is **NO** Competing Interest.

Cascading Impacts of AMOC weakening and collapse on Marine Biogeochemistry

Paul Lerner[1,2], Anastasia Romanou[1,2]

[1]Dept. of Applied Physics and Applied Mathematics, Columbia University, New York.

[2]NASA Goddard Institute for Space Studies, New York.

Key Points [up to 3; 140 characters or less]**:**

- The most severe responses include NPP collapse and deoxygenation in the subpolar North Atlantic, and a weakening carbon sink in the Arctic.
- Responses are rapid (<20 yr) due to teleconnections in impacts between the North Atlantic and Pacific, but slow (>100 yr) in the Southern Hemisphere.
- Impacts occur at a global warming level as low as 2.8℃, a threshold expected to be crossed under current emissions policies by 2100.

Guidelines for formatting: https://www.nature.com/nclimate/content
Submission guidelines: https://www.nature.com/nclimate/submission-guidelines

Abstract

As anthropogenic emissions continue to increase Earth's surface temperature, the Atlantic Meridional Overturning Circulation (AMOC) is at risk of weakening substantially and crossing a tipping point. Then, multiple Earth system components may be significantly and irreversibly altered. Here we investigate the responses of ocean carbon uptake, net primary productivity (NPP), oxygen concentration, and carbon storage to an AMOC collapse induced by extremes in the internal variability in the subpolar gyre under a moderate forcing scenario. While similar ensemble splitting has been found in other models, the NASA Goddard Institute for Space Studies (GISS) Earth system model (ESM) was the first to report an AMOC bifurcation due to internal variability, without the need to prescribe freshwater hosing. We find severe regional impacts, including collapsed NPP and deoxygenation in the subpolar North Atlantic, and reduced carbon uptake in the Arctic and subtropical North Atlantic. We identify the physical drivers of these ocean biogeochemical impacts and, for the first time, provide estimates of their lag and latency, i.e. the timescales over which these impacts begin to occur and are fully realized, respectively. Timescales are generally found to increase southward from the deep convection sites, but are remarkably similar between basins at similar latitudes.

Plain Language Summary

As greenhouse gas emissions increase global temperatures, a major network of ocean currents in the Atlantic—known as the AMOC—is at risk of shutting down. If this "conveyor belt" reaches a tipping point and collapses, it could permanently alter the Earth's environment. This study uses the NASA climate model to look at the ripple effects of an AMOC shutdown to the ocean's health. Notably, the model shows this collapse can be triggered by natural, extreme shifts in surface ocean freshening, even without the massive "meltwater" from glaciers that scientists usually assume is necessary. We find that an AMOC total collapse would put marine life at risk in the North Atlantic since it threatens the base of the food chain there, i.e. the primary productivity from phytoplankton. Oxygen levels would drop significantly in the North Atlantic, making it harder for marine life to survive. The Arctic and parts of the Atlantic would become much less effective at absorbing carbon dioxide from the atmosphere and storing it away for centuries. Our study also estimates how long it takes for these impacts to reach different parts of the world. While the changes start in the North, they spread south surprisingly fast, hitting the Atlantic and Pacific oceans at roughly the same time. If this Atlantic current fails, the ocean's ability to support life and store carbon may be severely and permanently damaged, with effects that ripple across the entire planet faster than we previously thought.

Introduction

As Earth's surface temperature continues to rise under continuing greenhouse gas emissions, the Earth system is at risk of crossing critical thresholds (tipping points) for several tipping systems[1]. One of these systems is the AMOC, which transports warm and saline water from the subtropics to subpolar North Atlantic, thereby modulating regional climate in the North Atlantic[2]. Upon reaching the Nordic and Labrador Seas, water advected with the AMOC cools, subducts and is subsequently transported southward to the Southern Ocean, where it is drawn

up to the surface by wind-driven upwelling near Antarctica[3]. The weakening and collapse of the AMOC have been shown to be associated with a colder North Atlantic and Arctic[4,5,6,7], warmer Southern Ocean, more extensive Arctic sea ice[3,7,8], and a southward shift of the ITCZ[4,10,11]. AMOC weakening has also been shown to result in reduced precipitation[12] and changes in sea level height[12]3

Cascading tipping points occur when an abrupt change in one element of the Earth system leads to abrupt changes in other elements[14]. For the Earth system components to be considered "tipped", they must have entered a new state, and the time-scale of recovery to the prior state must be much longer than the timescale to reach this new state[15,16]. Previous studies have found regional state changes in ocean biogeochemical properties in response to AMOC collapse. These include a reduction/enhancement of ocean carbon uptake in the Arctic and North Atlantic, respectively[17,18], as well as a decline in ocean net primary productivity (NPP)[19,20], suggesting some consistency in the direction of these responses in ocean biogeochemical models despite using hosing under different background climate states. However, the response of other ocean biogeochemical properties, such as ocean oxygen concentration, have only been investigated in a single model[19]. It is also unclear whether such responses are generalizable, since in all these models the collapse of AMOC is induced at different equilibrium or transient background states by freshwater hosing[21], which often involves too large a freshwater forcing and may not allow for all the feedbacks between ocean-ice-atmosphere to evolve before, during and after AMOC collapses. Furthermore, while changes in ocean biogeochemical properties under a collapsed AMOC have been investigated, their timescales, particularly how long they take to manifest themselves relative to AMOC collapsing, have not been examined.

The NASA-GISS ESM is known to have a bifurcation point where the effect of internal climate variability on AMOC may become stronger than the greenhouse forcing effect and cause the AMOC to collapse in a mid-range future forcing scenario (SSP2-4.5) around 2110 and without the need to prescribe external freshwater forcing (hosing, e.g. NASHOSMIP[7]). In the GISS SSP2-4.5 simulation, eight out of ten identically forced ensemble members under extended SSP2-4.5 CMIP6 forcing exhibited AMOC that recovered as the forcing declined (AMOC-on), while in two out of ten AMOC collapsed despite the forcing decline (AMOC-off). This stochastically induced AMOC bifurcation has been analyzed in ref.[22] It is noteworthy that such ensemble splitting (or ensemble divergence) has been henceforth identified in other models as well[23,24].

Here, we use the same physical model as in ref.[22], the E2.1 climate model (GISS-E2-1-G), coupled to the NASA-GISS ocean carbon cycle model (NOBMg[25,26,27,28]), to examine the response of various ocean biogeochemical properties under collapsed and recovered AMOC states. We focus on the air-sea exchange of CO_2, net primary productivity, intermediate water ocean oxygen concentration, and dissolved inorganic carbon storage. Our goal is to determine (i) which regions exhibit the largest changes in these properties under AMOC collapse, (ii) what are the magnitudes and directions of these changes, and (iii) what are the timescales at which these ocean biogeochemical properties begin responding to a collapsing AMOC and reach steady state. We distinguish two different timescales: the lagged response between the time AMOC bifurcation occurs and the time bifurcation occurs in the impacted fields (e.g. air-sea flux, carbon storage, NPP, deoxygenation etc) and the latency which is the timescale after the

AMOC bifurcation for the tipping behavior to fully materialize in the impacted field (i.e. reach quasi steady-state).

Results

Global Response

Analyzing the model response after 2070 and distinguishing the response in the ensemble members where AMOC collapses (AMOC-off) vs. those where the AMOC recovers (AMOC-on) (see methods; Extended Data Fig. 1), we find that there is strong coherency between AMOC at 48°N and AMOC at 26°N. All ensemble members show similar AMOC magnitude decline by 2100, followed by recovery in some ensemble members by around 2200 at levels ~1 Sv below the late historical (1980-2014; Figure 1a-c) and collapse (AMOC strength < 3 Sv) in the rest of the ensemble members. The AMOC bifurcation occurs at global mean surface air temperature (SAT) 2.2±0.1°C (Fig. 1d) above the late historical (a global warming level of 2.8±0.1), a level expected to be exceeded under current emissions policies by 2100[29]. Global mean SAT is substantially colder due to the collapsed AMOC by as much as 1.1°C by year 2320.

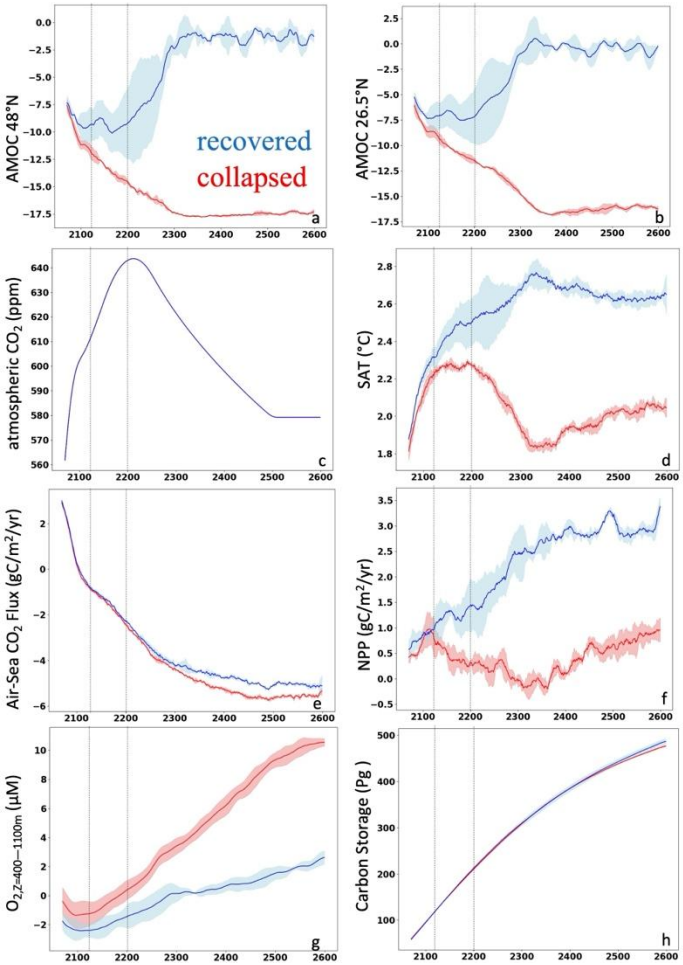


Fig. 1: (a) AMOC strength decline, shown as anomaly from the historical simulation's ensemble mean 1980-2014 climatology, at 48°N. Red (blue) curves and shading correspond to ensemble mean and 1-σ standard deviation of the members with collapsed (recovered) AMOC. (b) As in

(a), but for AMOC at 26.5°N, the location of the RAPID-MOCHA array measurements[30]. (c) Atmospheric CO_2 concentration for the SSP2-4.5 extension scenario, beginning in the year 2070. (d) As in (a), but for surface air temperature (area-weighted). (e) As in (a), but for global average air-sea flux of CO_2 (positive = into the ocean). (f) as in (a), but for global average ocean net primary productivity. (g) as in (a), but for mass-weighted globally averaged oxygen concentration between 400 and 1100 m. (h) as in (a), but for globally integrated carbon storage. The left-most vertical dashed line shows the time at which AMOC in collapsed and recovered ensemble members become significantly different from one another (1-σ apart, see Methods), while the second vertical dashed line shows the year of maximum atmospheric CO_2. For this and all remaining figures, time-series are smoothed using a 20-yr moving average filter. Extended Data Fig. 1 shows the same absolute time series (not anomalies).

Carbon uptake by the ocean as well as marine primary productivity and oxygen concentrations change little due to AMOC collapse (<5% of their late historical values; Fig. 1e-g, Extended Data Fig. 1a-c). The global ocean carbon sink as expressed by changes in the carbon storage (i.e. the inventory of its dominant contribution, DIC storage, below 1000 m) also shows no significant change (Fig. 1h, Extended Data Fig. 1d).

Cascading Tipping in Drivers and their Ocean Biogeochemical Impacts

While these global mean responses to AMOC collapse are small, regionally they are substantial (Fig. 2). The ocean absorbs CO_2 from the atmosphere much more efficiently in the North Atlantic and less so in the Greenland, Norwegian, and Iceland (GIN) Seas in the Arctic, and has no change in the Southern Ocean (Fig. 2a). Net primary productivity collapses in the North Atlantic while it shows a smaller but still statistically significant decline in the GIN sea region, and moderate increases in the South Atlantic and Southern Ocean (Fig. 2b). At intermediate ocean depths, where oxygen is not in contact with the atmosphere, oxygen concentration increases throughout the northern hemisphere, most acutely in the North Pacific and subtropical North Atlantic, but declines dramatically in the subpolar North Atlantic (Fig. 2c). The Arctic becomes a more potent carbon reservoir per unit area (Fig. 2d). However, since the Arctic is only a small fraction of the ocean's surface area, it does not contribute much to the globally integrated response (Fig. 1g).

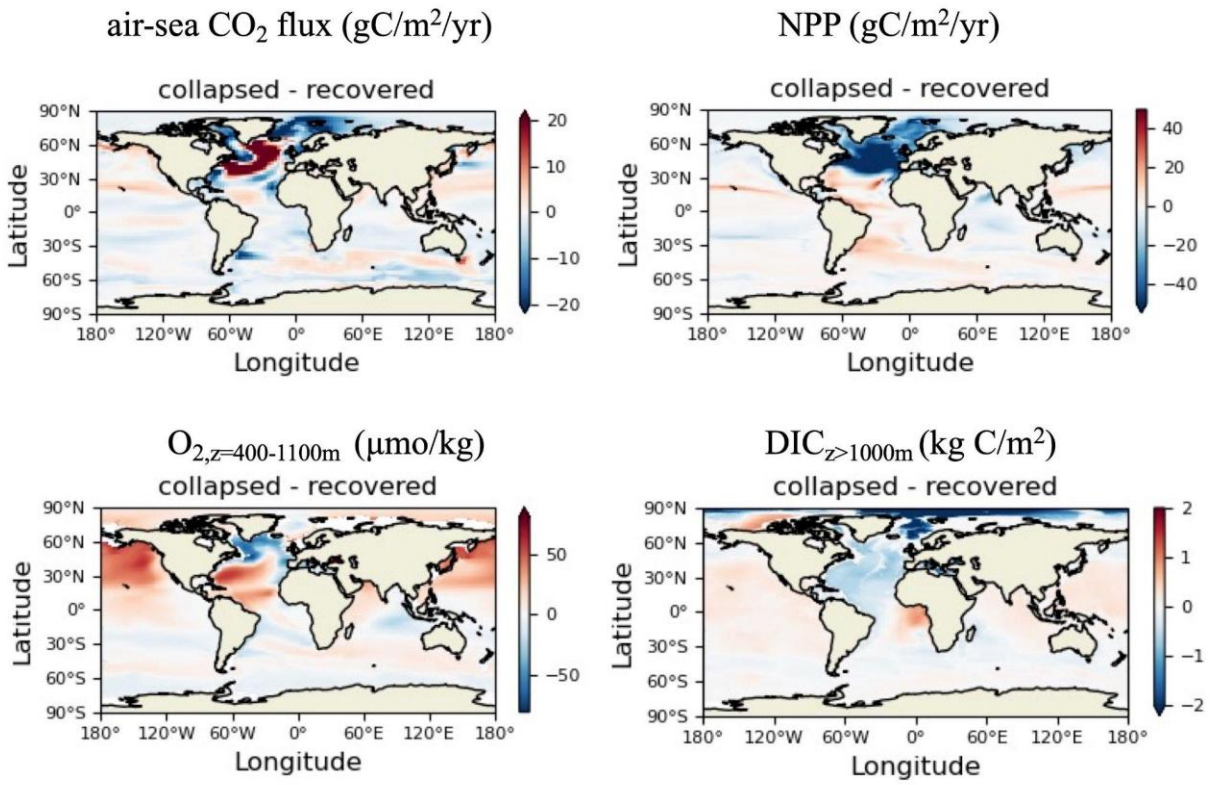


Fig. 2: Response of (a) the air-sea CO_2 flux, (b) NPP, (c) intermediate layer O_2, and (d) carbon storage to AMOC collapse biogeochemical properties to AMOC collapse. Responses are the difference between collapsed and recovered mean states averaged between the years 2350 and 2400.

Using the LASSO regression (see Methods), we can determine the lagged timescales of tipping in the drivers of these ocean biogeochemical responses. We find that they vary considerably between regions, ranging from decades or less in the northern high latitudes to centuries in the Southern Ocean (Fig. 3). Here, we focus on the regions (Extended Data Fig. 2) that either show the largest responses, or display unique response timescales (e.g., lagged compared to other regions) although all responses are provided in the Extended Data. An example of the cascading impacts of AMOC collapse and their lags is shown for the subtropical North Atlantic (Fig. 4), where impacts are most pronounced, and a summary of the lagged timescale is shown in Fig 5. An almost concurrent increase in carbon uptake (lag ~10 years) is driven mainly by intensifying winds as the AMOC collapses (Fig. 3, 4, 5), while the almost immediate response of NPP is driven equally by regional ocean cooling and lower nutrient availability responding to the shoaling mixed layer depths (Fig. 3, 4, 5, Extended Data Fig. 3a). SST cooling is consistent with reductions in poleward heat transport as AMOC slows down, as illustrated by multiple previous studies[8,31], while mixed layer depth shoaling is consistent with the collapse of deep convection in the subpolar North Atlantic. At slightly longer timescales (~50 yr) the intermediate ocean oxygenation response (Fig. 3, 4, 5) is driven by enhanced ventilation of intermediate waters caused by salinification of the upper ocean in the tropics and extratropics of the Atlantic, which increases the density, depth, and northward extent of mode waters from this region (Extended Data Fig. 3b,c). On longer timescales (~200 yr timescale)

carbon storage reduction (Fig. 3, 4) is driven by the reduced ventilation of deep water. In the subtropical North Atlantic, all properties except carbon storage show a latency of 2225-2275 yrs (Fig 3). Carbon storage continues to increase until the end of the simulation (Extended Data Fig. 2w).

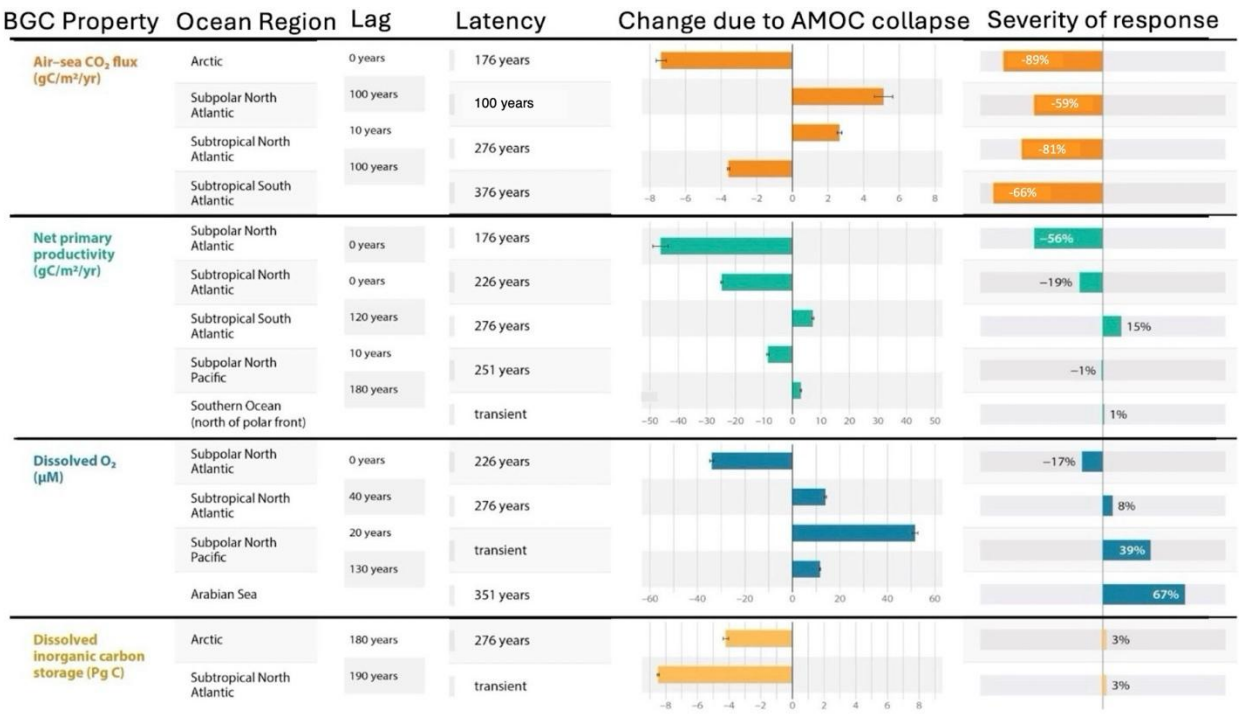


Fig. 3: Regional ocean biogeochemical responses and their timescales of lag and latency responses. For each ocean biogeochemical property and region, the lag is the time after the AMOC bifurcates when the property begins to exhibit a response (see Methods). The latency is the delay between when the AMOC begins to bifurcate and the property reaches a quasi-steady state for AMOC-off members. Change due to AMOC collapse is the difference between the AMOC-off and AMOC-on states at quasi-steady state. Severity of response is the difference in the property between the AMOC-off state and the late historical (1980-2014 climatology). Panels show differences between AMOC-on and AMOC-off responses for (a) the air-sea CO_2 flux ($gC/m^2/yr$), (b) NPP ($gC/m^2/yr$), (c) intermediate layer oxygen concentration (µM), and (d) carbon storage (Pg C). Differences are averaged over the 50 years after collapsed and recovered states have achieved a quasi-steady state. The numbers to the right of the bars show the latency when bifurcation occurs for each impact relative to the year AMOC bifurcates (2124). Image credit: Fiona Martin.

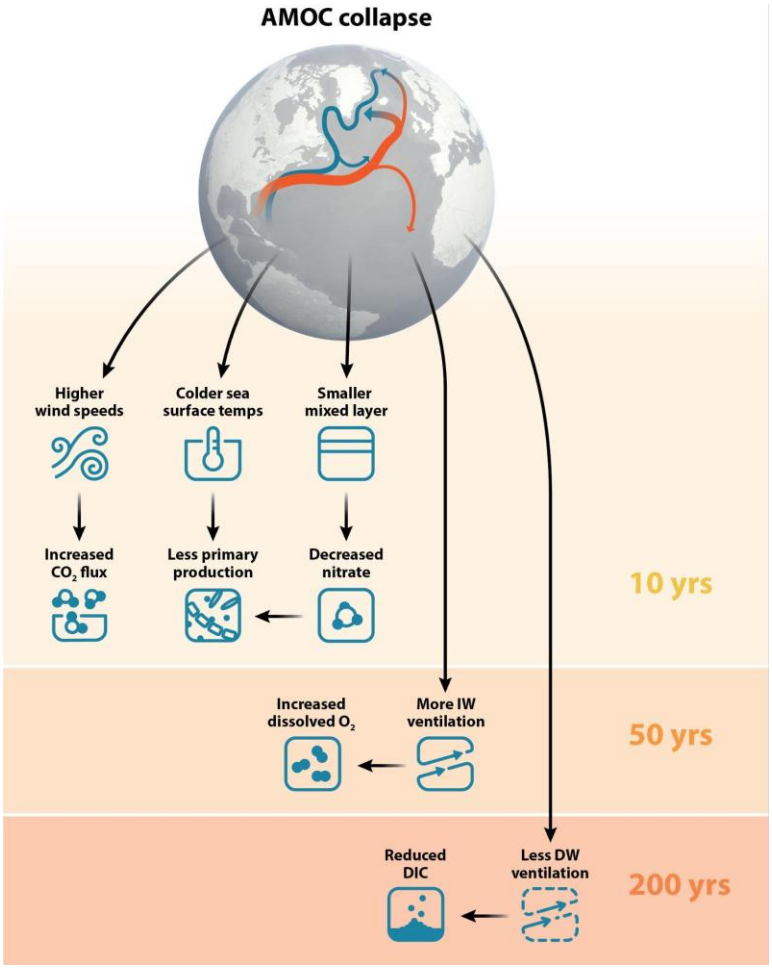


Fig. 4: Drivers of ocean biogeochemical responses to AMOC collapse in the **subtropical North Atlantic** and their lagged response (as described in Fig. 3). Timescales refer to lags in Fig. 3. Plots for the other basins are shown in Extended Data Fig. 4. Image credit: Fiona Martin.

With few exceptions, the lag between AMOC bifurcation and high-latitude ocean biogeochemical responses is small (<20 yrs) in the northern high latitudes (Fig. 3). Deoxygenation of subpolar North Atlantic intermediate waters is driven by reduced ventilation of intermediate waters (Extended Data Fig. 4a), while oxygenation of subpolar North Pacific intermediate waters is driven by increased ventilation (Extended Data Fig. 4b). The ventilation reduction is driven in the subpolar North Atlantic by the collapse of deep convection in the Irminger Sea, resulting in wintertime MLDs that are even shallower than in the subtropical North Atlantic (Extended Data Fig. 3a), and in the subpolar North Pacific by salinification and increased density of waters in the upper 500 m (Extended Data Fig. 3d,e). Colder sea surface temperature drives a productivity decline in both regions (Extended Data Fig. 4a,b), but the magnitude of decline is much larger in the subpolar North Atlantic (Fig. 3). The synchronicity of the NPP and O_2 responses to AMOC bifurcation suggests atmospheric teleconnections are responsible for propagating changes from the North Atlantic to the Pacific. Such teleconnections may include AMOC-collapse driven intensification of the Aleutian low[32], or an

increase in Arctic sea-ice presence which reduces atmospheric anomalies associated with air-sea heat transfer in the Arctic ocean that extend from the North Pacific to North Atlantic[33].

Sea-ice controls the CO_2 flux reduction in the Arctic and increase in the subpolar North Atlantic, but at different timescales. In the subpolar North Atlantic, the responses of the sea ice coverage and the flux lag the AMOC bifurcation by a century (Fig. 3, Extended Data Fig. 4a), while in the Arctic they occur synchronously with the AMOC bifurcation (Fig. 3, Extended Data Fig. 4c). An increase in subpolar North Atlantic sea-ice results from Arctic surface temperature declines due to the expansion of the warming hole induced by AMOC weakening and increases in sea-ice transport through the Denmark Strait[22]. Carbon storage lags AMOC bifurcation by almost a century in the Arctic (Fig. 3), with a decline driven by reduced deep water ventilation (Extended Data Fig. 4c). The largest changes due to AMOC collapse are also exhibited in the northern hemisphere, including a >50% NPP reduction in the subpolar North Atlantic, greatest oxygenation and deoxygenation in the subpolar North Atlantic and subpolar North Pacific respectively, and the largest CO_2 uptake reduction in the Arctic CO_2 (Fig. 3). Latencies are generally between 200-300 yrs, except for the much shorter (100 yrs) latency of the subpolar North Atlantic CO_2 flux.

Moving southward, the Arabian Sea only shows a statistically significant response in intermediate oxygen concentration (Extended Data Fig. 2t). It takes over 100 years for the lagged response to AMOC here (Fig. 3), and is driven by a reduction in the upward flux of deeper (>1100 m), older waters into the intermediate layer (Extended Data Fig. 4d, 5). The latency of the O_2 response is ~100 yrs longer than in the North Atlantic, but still shorter than in the subpolar North Pacific (Fig. 3). The O_2 change due to AMOC collapse is also smallest in this region.

In the subtropical South Atlantic, NPP takes over a century longer to respond to AMOC bifurcation than in the northern hemisphere (Fig. 3), while the CO_2 uptake takes a century longer than in the subtropical North Atlantic and Arctic, but responds almost at the same time as the subpolar North Atlantic. Increased surface ocean pCO_2 (Extended Data Fig. 4e), driven by increased temperature, salinity, and DIC (Extended Data Fig. 6), controls the reduction in CO_2 flux in the South Atlantic. Warmer SSTs also drive the NPP response in the southern hemisphere, along with increased surface iron concentration (Extended Data Fig. 4e). NPP increases in the Southern Ocean are also driven by SST (Extended Data Fig. 4e), but with an even more lagged response (180 yrs; Fig. 3). Southern Hemisphere SST and SAT increases, which have lagged responses to AMOC bifurcation like that of NPP (Extended Data Fig. 7c,d,i,k), are consistent with the bipolar seesaw hypothesis, where as AMOC weakens, heat that would have otherwise been exported to the North Atlantic is left to accumulate in the South Atlantic, raising the temperatures there[34,35]. The latency of the CO_2 flux and NPP is a century longer in the subtropical South vs. North Atlantic (Fig. 3).

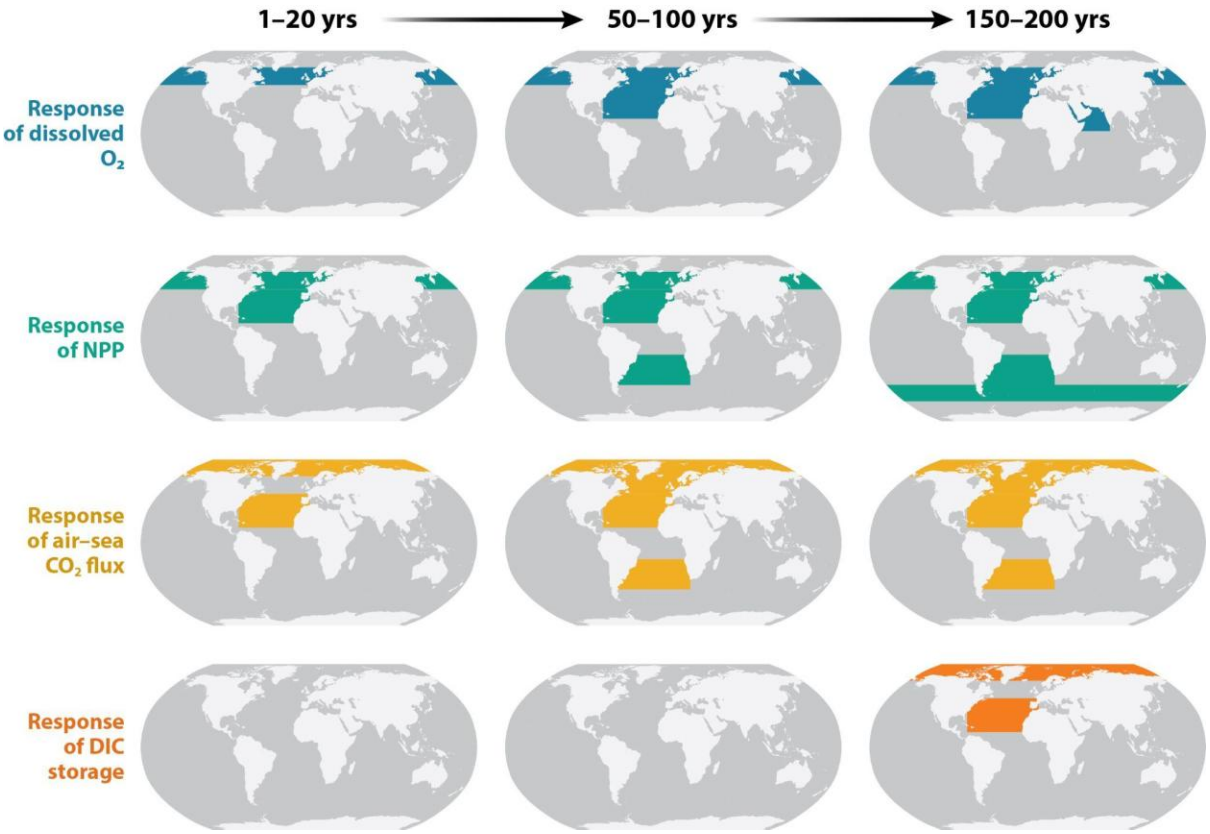


Fig. 5: Lag timescales of ocean biogeochemical cascades after the AMOC bifurcates. Rows are biogeochemical properties, columns are years in which these properties exhibit bifurcation of the collapsed and recovered ensemble means, relative to the year of AMOC bifurcation (2124). Image credit: Fiona Martin.

Discussion

We find that consequences of AMOC collapse can be regionally severe even if globally muted. While previous numerical studies have investigated the response of ocean biogeochemistry to AMOC collapse, comparison to these studies may be difficult due to (i) AMOC collapse occurring at different global warming levels, as it has been shown that climate responses are state-dependent[36], (ii) different amounts of freshwater forcing being used, while in our study there is no external freshwater forcing, and (iii) responses being analyzed at different timescales.

For example, different studies prescribe vastly different amounts of freshwater forcing ranging from $2x10^{-4}$ Sv/yr to 1 Sv/yr[17, 18,19,20] over different periods of time and under different background state (e.g. pre-industrial background climate[17,19], or future climates[18,20]) and examined responses after different time horizons, with few focusing on quasi-steady state[19]. Consequently, some studies found an increase in the subpolar North Atlantic and reduction in the Arctic CO_2 flux due to AMOC collapse[17] similar in magnitude to that found in our study, while others found changes in the CO_2 flux of the same sign, but roughly half the magnitude[18]. Changes under SSP5-8.5 forcing suggest a reduced impact of AMOC collapse with warmer

background climates[18], but this relationship has yet to be verified in other models. Our North Atlantic and Arctic NPP declines are consistent with previous studies[19,20], but the South Atlantic response is debatable[19,20]. As for the CO_2 flux, one model found the NPP response to be reduced with increased background warming[20]. The deoxygenation in the subpolar North Atlantic in our model is 30-50% less severe than previously estimated[19], and our model also simulates a ~20% weaker oxygenation in the subpolar North Pacific.

Despite differences in the magnitudes of change, increased carbon uptake in the subpolar North Atlantic, collapse in NPP in the North Atlantic, and a dramatic (>50 umol/kg) deoxygenation in the subpolar North Atlantic and oxygenation in the North Pacific have been consistently found here and in these previous studies. The consistency in direction of the biogeochemical impacts suggests these are properties that are at risk if AMOC collapses under continued anthropogenic forcing which, despite not having a high likelihood[16], some studies suggest may happen as early as the mid-21st century[37,38].

Our study, in contrast to previous modelling efforts, also provides estimates of the lag and latency of the impacts, i.e. the timescales at which impacts begin to respond to an AMOC collapse and reach quasi-steady state. Particularly for NPP, the lagged responses are abrupt (within 10 years of collapse) in the northern hemisphere, and in the case of subpolar North Atlantic deoxygenation, they are still within decadal timescales (~50 yrs). The latency of all properties is over a century, and we find that, just as the AMOC does not recover for at least two centuries after a complete collapse, severe deoxygenation or NPP collapse show no signs of recovery. Finally, it should be emphasized that, in contrast to previous studies, in our simulations AMOC collapses in response to internal dynamics and under a mid-range scenario, nowadays plausible scenario, for future CO_2 forcing.

Our results show severe regional decline in ocean carbon uptake (Arctic and subtropical North Atlantic), NPP (North Atlantic), and O_2 (subpolar North Atlantic) relative to present-day values (Fig. 3). In addition to collapsing NPP, previous studies have shown a shift in phytoplankton community composition in the subpolar North Atlantic, with an increase in small phytoplankton and reduction in diatoms and diazotrophs[20,39]. Previous studies[20] also found a significant reduction in the biomass of commercial species when forcing an AMOC collapse. Our model agrees with previous studies that there are changes in community composition. Assuming these impacts happen synchronously with NPP, a collapsing AMOC would have almost immediate consequences for commercial fisheries. There may also be compounding effects of AMOC collapse on pelagic fish in the high-latitude North Atlantic decades after AMOC begins collapsing, as both prey availability and well-oxygenated habitats are diminished[40].

Placing our findings in the context of paleoclimate evidence may be highly debatable, because of the difference in the background climate with present day climate, but might also be informative. AMOC has been suggested to have undergone substantial weakening or collapse under Heinrich Stadials[41,42]. Paleo-reconstructions of 700-800 m oxygen concentrations in the eastern tropical Atlantic and Arabian Sea suggest oxygenation during HS1[43,44], which is consistent with the enhanced intermediate layer oxygen concentration we find in these regions under AMOC collapse. Our finding of a severe reduction in North Atlantic NPP is also consistent with paleo-records between 40°N and 63°N of a general decrease in diatom accumulation during HS1 and HS4[45]. Multi-proxy reconstructions of NPP from sediment cores in the South Atlantic, Pacific and Atlantic sectors of the Southern Ocean, and Eastern Tropical North Pacific[46]

also indicate increased NPP during Heinrich events, consistent with increased NPP in these regions found during AMOC collapse in our study. Additionally, the ~200 yr SST lag between the North Atlantic and Southern Ocean shown here is remarkably consistent in terms of the lag between temperature records in Greenland and West Antarctic Ice sheet cores[47]. However, not all paleo-proxy evidence suggests the same direction of NPP change during Heinrich events, with $\delta^{13}C$ in multiple sectors of the southern hemisphere suggesting reduced productivity during HS1[48]. Moreover, whether there should be similar changes in biogeochemical properties during AMOC collapse under cold and warm background climates remains unclear.

Despite the limitations of comparing our results to the aforementioned paleoproxies, our study is the first to provide regional timescales of ocean biogeochemical properties to AMOC collapse. Our findings suggest that adaptation measures would be useful if implemented prior to AMOC collapse, given how rapid cascading impacts can occur. Our study shows the cascading effects of a collapsing AMOC may occur at a global warming level of 2.8℃, which can occur by the end of the century if we follow current emissions trajectories[29]. However, we emphasize that single model results have large uncertainties, and therefore intercomparison studies following protocols such as the TIPMIP and TIPESM[49,50] will allow us to better constrain these timescales.

Methods

2.1 *Model Configuration*

We analyze 10 identically forced ensemble members of the ocean carbon cycle and AMOC response to the extended Shared Socioeconomic Pathway (SSP) 2-4.5[51] greenhouse gas (GHG) emissions and mitigation scenario, in the NASA Goddard Institute for Space Studies (GISS) version E2.1 climate model (GISS-E2-1-G). These simulations were part of the official submission of the NASA GISS climate group to the Climate Model Intercomparison Project phase 6 (CMIP6)[52]. The atmospheric component of GISS ModelE has 2° by 2.5° latitude and longitude resolution respectively, 40 vertical layers and a model top at 0.1 hPa. The ocean component, GISS Ocean v1, is mass conserving with a free surface, natural surface boundary conditions for heat and freshwater fluxes[53], horizontal resolution of 1° by 1.25° in latitude and longitude, respectively, and 40 vertical layers[54]. The GISS Ocean v1 model has 5 to 20 m resolution in the seasonal mixed layer, 20 to 80 m resolution in the thermocline and 100–200 m at depths greater than 1000 m. Heat, salt, and tracers are advected by the quadratic upstream scheme[55] and are vertically mixed by the K-profile parameterization (KPP[56]). Eddy related fluxes by mesoscale baroclinic turbulence are parameterized following the Gent-McWilliams parameterization (GM[57]) with variable coefficients[58] where mesoscale transport is expressed in local quasi-isopycnal layering, and the vertical diffusivity includes a contribution from tidal dissipation which mostly impacts the shallow water regions bordering the North Atlantic. Ventilation of marginal seas has been increased by slight tuning of the strait depths and by

increased horizontal diffusivity locally. Previous sensitivity studies[58,59] showed good agreement with observations with regards to uptake of passive tracers.

The sea ice component has two mass layers and two thermal layers in each mass layer. The sea ice dynamics is based on a formulation of the viscous-plastic rheology[60] and the sea ice thermodynamics uses the "brine-pocket" parameterization[61,62] that allows salt to play a more active role in the specific heat and melt rates of sea ice. Processes relevant to the salt budget (e.g., gravity drainage and flushing of meltwater) are consistently treated with the brine pocket physics.

Ocean biology and chemistry are simulated by NASA-GISS Ocean Biogeochemical Model (NOBMg[25,26,27,28,63]). A brief overview of NOBMg is provided in this section, while a more detailed description and evaluation can be found in ref[64]. NOBMg includes four phytoplankton functional groups (diatoms, chlorophytes, cyanobacteria, and coccolithophores), three detrital pools (POC, detrital silica, and detrital iron), four nutrients (nitrate, ammonia, silicate, and iron), one heterotrophic species, dissolved organic carbon (DOC), dissolved inorganic carbon (DIC), dissolved oxygen and alkalinity. Dissolved oxygen and DIC interact with atmospheric O_2 and CO_2, respectively, through parameterized gas exchange following the CMIP6 protocol[65]. Light profiles from the atmospheric radiation module are extended into the ocean and spectrally decomposed to 33 wavebands that are used to compute growth of the phytoplankton groups, sinking profiles, as well as changes in the vertical distribution of ocean temperatures due to biologically mediated absorption and scattering in the water column[27,66]. The ocean iron cycle is forced with a monthly climatology of dust deposition calculated offline by ModelE, with the soluble fraction equal to 2% of the deposited mass[25]. The concentrations of DOC, DIC, nitrate, silicate and Fe for all the major and many minor rivers are prescribed from an annual climatology[67], which determines the biogeochemical composition of the freshwater outflow at these sites. Air-sea carbon fluxes, nutrients, oxygen, and primary productivity have been assessed against observations from SOCAT, GLODAPv2, and SeaWiFS/MODIS-AQUA, respectively[26]. More recently, the iron cycle in ModelE has been improved through the inclusion of prescribed ligands and a significant increase in the rate of ligand-bound iron scavenging to be consistent with observed rates for trace metals with similar scavenging characteristics as iron[64].

2.2 *SSP2-4.5: Ensemble Simulations and AMOC bifurcation*

A pre-industrial control of the coupled atmosphere-ocean of E2.1 was spun-up for 7892 years to obtain equilibrium conditions for the physical system, i.e. the top of the atmosphere radiative imbalance is zero. After year 7500, the carbon cycle was enabled and the entire Earth system model was spun-up for 392 years under preindustrial forcings. Carbon cycle equilibrium conditions are attained with air-sea flux, land uptake and total carbon uptake all being zero. At that point, 10 ensemble member simulations of the historical period 1850-2014 were launched from the pre-industrial control run at 20-year increments, with the first 20-year increment beginning at year 7842. Ensemble simulations for SSP2-4.5 were continued after each ensemble member reached the year 2014. The nominal radiative forcing for SSP2-4.5 represents a "middle-of-the-road" scenario that continues the forcing patterns of the late-historical simulation after 2014 in terms of anthropogenic emissions and developments in environmental systems. The forcing increases near-linearly to year 2100, increases but at a reduced rate till

year 2200[51], and then decreases linearly from year 2200 to year 2500, flattening out after year 2500 (Figure 1c).

AMOC at 48°N and 26°N (Fig. 1a,b and Extended Data Fig. 8) shows a bifurcation around the year 2124, which is the time when the difference between the ensemble-mean of the members that exhibit AMOC collapse and those that show AMOC recovery becomes significant (at the ± 1-σ level). Bifurcations in other variables are similarly identified for the biogeochemical properties examined in this study.

We identify ensemble members with a collapsed AMOC as those in which AMOC reaches a magnitude of less than 3 Sv at 48°N (less than 6 Sv at 26°N, following previous studies[7]) for a period of at least 100 yrs. We find that members c, g, and i show a near-complete collapse after year 2300, with members a, b, and d showing a corresponding recovery during the same period (Extended Data Fig. 8). The ensemble mean and standard deviation of all variables reported in this study are computed separately for members that recover (a,b,d) and collapse (c,g,i).

2.3 *Definition of Regions*

Minimum-maximum latitude and longitude bands used to defined regions are as follows. The subtropical North Atlantic (15°N-45°N, 75°W-0°E), the subpolar North Atlantic (45°N-60°N, 75°W-30°E), the subtropical South Atlantic (45°S-15°S, 65°W-15°E), the Southern Ocean North of the Polar Front (65°S-45°S, 180°E-180°W), and subpolar North Pacific (45°N-65°N, 140°E-110°W), the Arabian Sea (0°N-24.5°N, 45°E-75°W), and the Arctic (65°N-90°N, 180°W-180°E).

2.4 *Identification of Drivers*

We use a Least Absolute Shrinkage and Selection Operator (LASSO) Regression to determine the dominant drivers to the ocean biogeochemical responses to AMOC collapse in each region, which has the advantage of identifying the most important drivers even in the presence of high multicollinearity between regressors[68]. Given a linear regression with predictors $x_{i,j}$ and response values y_i for $i=1..N$ and $j=1…p$, where N is the number of samples and p is the number of predictors, the lasso solves the regression problem of finding $\widehat{\beta_j}$ that minimizes (Tibshirani 2011):

$$\sum_i (y_i - \sum_j x_{ij}\beta_j)^2 + \lambda \sum_j |\beta_j|$$

Where λ is a penalty parameter that acts to shrink the absolute magnitude of the regression coefficients such that only a subset of the initial regressors are needed to explain the variance in the variable being predicted (*y*). The regressors chosen for each variable are those we think encapsulate the range of processes that can drive significant changes are AMOC collapse. They include sea-ice, the air-sea pCO_2 gradient, and wind speed for the CO_2 flux, SST, nitrate, iron, for NPP, potential temperature, carbon export at 400 m, and ventilation (as quantified by an ocean age tracer averaged between 400-1100 m) for intermediate layer oxygen concentration, and potential temperature, respired carbon (below 1000 m), and ventilation (again quantified by the age tracer, but now average below 1000 m). Respired carbon is calculated using apparent oxygen utilization, as in previous studies[69].

The regression models are such that the predicted variable is the ocean biogeochemical property difference between the collapsed and recovered ensemble mean, and the regressors are also differences between the collapsed and recovered ensemble means. Regression coefficients are obtained using data between the year of AMOC bifurcation (2124) and the year at which the AMOC reaches a fully collapsed state (year 2300). Fits of the LASSO regression to the simulated data are presented in Extended Data Fig. 9: in all cases $r^2 > 0.8$. Once the regression coefficients are obtained, we use them to attribute the fraction of the difference in the ocean biogeochemical property between the collapsed and recovered ensemble means averaged between 2350-2400, during the fully collapsed state. As an example, we attribute the difference in NPP as:

$$\Delta NPP_{2350\text{-}2400} = \beta_{SST}\,\Delta SST_{2350\text{-}2400} + \beta_{Nitrate}\Delta Nitrate_{2350\text{-}2400} + \beta_{Iron}\Delta Iron_{2350\text{-}2400} \quad (2)$$

Where the regression coefficients are obtained from the LASSO regression. Note that there is no y-intercept in the regression model because the predicted variable and regressors are centered prior to regression. Each term on the right of eq. 2 is considered a contribution to the change in NPP between the collapsed and recovered runs. Contributions of each of the regressors to the changes in ocean biogeochemical properties between collapsed and recovered runs are shown in Extended Data Fig. 10.

To obtain uncertainties in our regression parameters, we use resampling with replacement, using 100 iterations of random resampling of the regression data, and perform the LASSO regression each iteration. This results in a distribution of 100 regression coefficients for each regressor, from which we take the mean and standard deviation. For each iteration, 5-fold cross validation is used to estimate the penalty parameter. Finally, to obtain the uncertainties in each term in (2), we propagate the uncertainties based on the standard deviation of the 3 ensemble members with the uncertainties in the regression coefficient (e.g., $\beta_{SST}\,(\Delta SST_{2350\text{-}2400})_{err} = \beta_{SST}\,\Delta SST_{2350\text{-}2400}\sqrt{((\beta_{SST,err}/\beta_{SST,})^2 + (\Delta SST_{2350\text{-}2400,err}/\Delta SST_{2350\text{-}2400,})^2)}$

2.5 Estimation timescales, change due to collapse, and severity for each impact

The lag timescale, over which a given cascading impact following an AMOC collapse appears in any region, is estimated as the difference between the AMOC bifurcation time (2124) and the impact bifurcation time. The bifurcation time is estimated as the time when the difference in response between the ensemble members with AMOC-off and those with AMOC-on exceeds 1-σ. These timescales are depicted in all timeseries figures (Extended Data Fig. 2,7) with vertical dashed lines; the left-most vertical line is the bifurcation timescale of the AMOC and the right-most line is the lagged timescale of the response. The latency timescale, over which a given cascading impact following an AMOC collapse is fully realized[49,70], is estimated as the difference between AMOC bifurcation and the time in which the collapsed property reaches a quasi-steady state. The change due to AMOC collapse is defined as the difference between BGC properties in the AMOC-off and AMOC-on quasi-steady states. Quasi-steady state is determined by visual inspection of collapsed and recovered properties (Extended Fig. 2). The severity is

484 defined as the relative difference (%) between BGC properties in the AMOC-off quasi-steady
485 state and the historical mean (1990-2014). All timescales, changes due to AMOC collapse, and
486 severities for regions examined in this study are shown in Fig. 3.

487

488 **Data and Code availability**
489 All GISS ModelE components are open source and available at
490 https://www.giss.nasa.gov/tools/modelE/. Source code as well as scripts and data used to
491 produce the analysis and results in this paper are available on zenodo (doi:
492 10.5281/zenodo.18883081[71]).

493 **Acknowledgments**
494 Computational resources were provided by the NASA Center for Climate Simulation High-End
495 Computing (HEC) Program through the NASA Center for Climate Simulation (NCCS) at Goddard
496 Space Flight Center. Climate modeling at GISS is supported by the NASA Modeling, Analysis and
497 Prediction program. The authors wish to thank Fiona Martin at Visualizing Science for the
498 graphics. Funding is provided from NASA-MAP Arctic (Cryo2023) 23-MAP23-0019 (PI
499 Romanou).
500

501

502

503

504

505

506

507

508

509

510

511

512

513

514

515 **References**

516 1. Armstrong McKay, D. I., Staal, A., Abrams, J. F., Winkelmann, R., Sakschewski, B., Loriani, S.,

517 et al. . (2022). Exceeding 1.5 C global warming could trigger multiple climate tipping points.

518 *Science*, *377* (6611). DOI: 10.1126/science.abn795

519 2. Buckley, M. W., & Marshall, J. (2016). Observations, inferences, and mechanisms of the

520 Atlantic Meridional Overturning Circulation: A review. *Reviews of Geophysics*, *54*(1), 5-63.

521 https://doi.org/10.1002/2015RG000493

522 3. Marshall, J., & Speer, K. (2012). Closure of the meridional overturning circulation through

523 Southern Ocean upwelling. *Nature geoscience*, *5*(3), 171-180.

524 https://doi.org/10.1038/ngeo1391

525 4. Vellinga, M., Wood, R. A., & Gregory, J. M. (2002). Processes governing the recovery of a

526 perturbed thermohaline circulation in HadCM3. *Journal of Climate*, *15*(7), 764-780.

527 https://doi.org/10.1175/1520-0442(2002)015<0764:PGTROA>2.0.CO;2

528 5. Levermann, A., Bamber, J. L., Drijfhout, S., Ganopolski, A., Haeberli, W., Harris, N. R., et. al..

529 (2012). Potential climatic transitions with profound impact on Europe: Review of the current

530 state of six 'tipping elements of the climate system'. *Climatic Change*, *110*(3), 845-878.

531 https://doi.org/10.1007/s10584-011-0126-5

532 6. Sgubin, G., Swingedouw, D., Drijfhout, S., Mary, Y., & Bennabi, A. (2017). Abrupt cooling over

533 the North Atlantic in modern climate models. *Nature communications*, *8*(1), 14375.

534 https://doi.org/10.1038/ncomms14375

7. Jackson, L. C., Alastrué de Asenjo, E., Bellomo, K., Danabasoglu, G., Haak, H., Hu, A., Jungclaus, J., Lee, W., Meccia, V. L., Saenko, O., Shao, A., & Swingedouw, D. (2023). Understanding AMOC stability: The North Atlantic hosing model intercomparison project. *Geoscientific Model Development*, *16*(7), 1975-1995. https://doi.org/10.5194/gmd-16-1975-2023

8. Drijfhout, S., Bathiany, S., Beaulieu, C., Brovkin, V., Claussen, M., Huntingford, C., et al. (2015). Catalogue of abrupt shifts in Intergovernmental Panel on Climate Change climate models. *Proceedings of the National Academy of Sciences*, *112*(43), E5777-E5786. https://doi.org/10.1073/pnas.1511451112

9. Liu, W., Xie, S. P., Liu, Z., & Zhu, J. (2017). Overlooked possibility of a collapsed Atlantic Meridional Overturning Circulation in warming climate. *Science Advances*, *3*(1), 1-7. DOI: 10.1126/sciadv.1601

10. Zhang, R., & Delworth, T. L. (2005). Simulated tropical response to a substantial weakening of the Atlantic thermohaline circulation. *Journal of climate*, *18*(12), 1853-1860. https://doi.org/10.1175/JCLI3460.1

11. Schneider, T., Bischoff, T., & Haug, G. H. (2014). Migrations and dynamics of the intertropical convergence zone. *nature*, *513*(7516), 45-53. https://doi.org/10.1038/nature13636

12. Ben-Yami, M., Blaschke, L., Bathiany, S., & Boers, N. (2024). No critical slowing down in the Atlantic Overturning Circulation in historical CMIP6 simulations. *EGUsphere*, *2024*, 1-38, https://doi.org/10.5194/egusphere-2024-1106

13. Levermann, A., Griesel, A., Hofmann, M., Montoya, M., & Rahmstorf, S. (2005). Dynamic sea level changes following changes in the thermohaline circulation. *Climate Dynamics*, *24*(4), 347-354. https://doi.org/10.1007/s00382-004-0505-y

14. Wunderling, N., von der Heydt, A. S., Aksenov, Y., Barker, S., Bastiaansen, R., Brovkin, V., et al (2024). Climate tipping point interactions and cascades: a review. *Earth System Dynamics*, *15*(1), 41-74. https://doi.org/10.5194/esd-15-41-2024

15. Brovkin, V., Brook, E., Williams, J. W., Bathiany, S., Lenton, T. M., Barton, M., et al. (2021). Past abrupt changes, tipping points and cascading impacts in the Earth system. *Nature Geoscience*, *14*(8), 550-558. https://doi.org/10.1038/s41561-021-00790-5

16. IPCC, 2021: *Climate Change 2021: The Physical Science Basis. Contribution of Working Group I to the Sixth Assessment Report of the Intergovernmental Panel on Climate Change* [Masson-Delmotte, V., P. Zhai, A. Pirani, S.L. Connors, C. Péan, S. Berger, N. Caud, Y. Chen, L. Goldfarb, M.I. Gomis, M. Huang, K. Leitzell, E. Lonnoy, J.B.R. Matthews, T.K. Maycock, T. Waterfield, O. Yelekçi, R. Yu, and B. Zhou (eds.)]. Cambridge University Press, Cambridge, United Kingdom and New York, NY, USA, 2391 pp. doi:10.1017/9781009157896.

17. Obata, A. (2007). Climate–carbon cycle model response to freshwater discharge into the North Atlantic. *Journal of Climate*, *20*(24), 5962-5976. https://doi.org/10.1175/2007JCLI1808.1

18. Boot, A. A., von der Heydt, A. S., & Dijkstra, H. A. (2024). Response of atmospheric pCO 2 to a strong AMOC weakening under low and high emission scenarios. *Climate Dynamics*, *62*(8), 7559-7574. https://doi.org/10.1007/s00382-024-07295-y

19. Brown, N., & Galbraith, E. D. (2016). Hosed vs. unhosed: interruptions of the Atlantic Meridional Overturning Circulation in a global coupled model, with and without freshwater forcing. *Climate of the Past*, *12*(8), 1663-1679. https://doi.org/10.5194/cp-12-1663-2016

20. Boot, A. A., Steenbeek, J., Coll, M., von der Heydt, A. S., & Dijkstra, H. A. (2025). Global marine ecosystem response to a strong AMOC weakening under low and high future emission scenarios. *Earth's Future*, *13*(1), e2024EF004741. https://doi.org/10.1029/2024EF004741

21. Rahmstorf, S., Box, J. E., Feulner, G., Mann, M. E., Robinson, A., Rutherford, S., & Schaffernicht, E. J. (2015). Exceptional twentieth-century slowdown in Atlantic Ocean overturning circulation. *Nature climate change*, *5*(5), 475-480.

22. Romanou, A., Rind, D., Jonas, J., Miller, R., Kelley, M., Russell, G., et al. (2023). Stochastic bifurcation of the North Atlantic circulation under a midrange future climate scenario with the NASA-GISS ModelE. *Journal of Climate*, *36*(18), 6141-6161. https://doi.org/10.1175/JCLI-D-22-0536.1

23. Gu, Q., Gervais, M., Danabasoglu, G., Kim, W. M., Castruccio, F., Maroon, E., & Xie, S. P. (2024). Wide range of possible trajectories of North Atlantic climate in a warming world. *Nature communications*, *15*(1), 4221. ttps://doi.org/10.1038/s41467-024-48401-2

24. Oh, J. H., Kug, J. S., Shin, Y., Geng, X., Wang, S., Jin, F. F., An, S.L., Xie, S.P., & Liu, W. (2025). Noise-induced tipping of Atlantic Meridional Overturning Circulation under climate mitigation scenarios. *Nature communications*.

25. Lerner, P., Romanou, A., Kelley, M., Romanski, J., Ruedy, R., & Russell, G. (2021). Drivers of air-sea CO2 flux seasonality and its long-term changes in the NASA-GISS model CMIP6

submission. *Journal of Advances in Modeling Earth Systems*, *13*(2), e2019MS002028. https://doi.org/10.1029/2019MS002028

26. Lerner, P., Romanou, A., Nicholson, D., Kelley, M., Ruedy, R., & Russell, G. (2024). The sensitivity of the equatorial pacific ODZ to particulate organic matter remineralization in a climate model under pre-industrial conditions. *Ocean Modelling*, *188*, 102303. https://doi.org/10.1016/j.ocemod.2023.102303

27. Romanou, A., Gregg, W. W., Romanski, J., Kelley, M., Bleck, R., Healy, R., et al. (2013). Natural air–sea flux of CO2 in simulations of the NASA-GISS climate model: Sensitivity to the physical ocean model formulation. *Ocean Modelling*, *66*, 26-44. https://doi.org/10.1016/j.ocemod.2013.01.008

28. Romanou, A., Romanski, J., & Gregg, W. W. (2014). Natural ocean carbon cycle sensitivity to parameterizations of the recycling in a climate model. *Biogeosciences*, *11*(4), 1137-1154. https://doi.org/10.5194/bg-11-1137-2014

29. van Vuuren, D., O'Neill, B., Tebaldi, C., Chini, L., Friedlingstein, P., Hasegawa, T., Riahi, K., Sanderson, B., Govindasamy, B., Bauer, N., Eyring, V., Fall, C., Frieler, K., Gidden, M., Gohar, L., Jones, A., King, A., Knutti, R., Kriegler, E., Lawrence, P., Lennard, C., Lowe, J., Mathison, C., Mehmood, S., Prado, L., Zhang, Q., Rose, S., Ruane, A., Schleussner, C-F., Seferian, R., Sillmann, J., Smith, C., Sörensson, A., Panickal, S., Tachiiri, K., Vaughan, N., Vishwanathan, S., Yokohata, T. & Ziehn, T. (in review). The scenario model intercomparison project for CMIP7 (scenariomip-CMIP7). *EGUsphere*, *2025*, 1-38 [preprint]. https://doi.org/10.5194/egusphere-2024-3765

30. McCarthy, G. D., Brown, P. J., Flagg, C. N., Goni, G., Houpert, L., Hughes, C. W., ... & Smeed, D. A. (2020). Sustainable observations of the AMOC: methodology and technology. *Reviews of Geophysics*, *58*(1), 1-34. https://doi.org/10.1029/2019RG000654

31. Jackson, L. C., Kahana, R., Graham, T., Ringer, M. A., Woollings, T. V. M. J., Mecking, J. V., & Wood, R. A. (2015). Global and European climate impacts of a slowdown of the AMOC in a high resolution GCM. *Climate dynamics*, *45*(11), 3299-3316. https://doi.org/10.1007/s00382-015-2540-2

32. Gong, X., Lembke-Jene, L., Lohmann, G., Knorr, G., Tiedemann, R., Zou, J. J., & Shi, X. F. (2019). Enhanced North Pacific deep-ocean stratification by stronger intermediate water formation during Heinrich Stadial 1. *Nature communications*, *10*(1), 1-8. https://doi.org/10.1038/s41467-019-08606-2

33. Joh, Y., Yeh, S. W., Delworth, T. L., Labe, Z. M., Wittenberg, A. T., Cooke, W. F., ... & Park, Y. G. (2026). Evolving synchronization of the Gulf Stream and Kuroshio-Oyashio Extension in a changing climate. *Science Advances*, *12*(8), 1-3. doi: 10.1126/sciadv.adx6366

34. Stocker, T. F., & Johnsen, S. J. (2003). A minimum thermodynamic model for the bipolar seesaw. *Paleoceanography*, *18*(4). https://doi.org/10.1029/2003PA000920

35. Pedro, J. B., Jochum, M., Buizert, C., He, F., Barker, S., & Rasmussen, S. O. (2018). Beyond the bipolar seesaw: Toward a process understanding of interhemispheric coupling. *Quaternary Science Reviews*, *192*, 27-46. https://doi.org/10.1016/j.quascirev.2018.05.005

36. Bellomo, K., & Mehling, O. (2024). Impacts and state-dependence of AMOC weakening in a warming climate. *Geophysical research letters*, *51*(10), 1-10. https://doi.org/10.1029/2023GL107624

639 37. Boers, N., Ghil, M., & Stocker, T. F. (2022). Theoretical and paleoclimatic evidence for abrupt
640 transitions in the Earth system. *Environmental Research Letters*, *17*(9), 093006. doi:
641 10.1088/1748-9326/ac8944
642 38. Ditlevsen, P., & Ditlevsen, S. (2023). Warning of a forthcoming collapse of the Atlantic
643 meridional overturning circulation. *Nature Communications*, *14*(1), 1-12.
644 https://doi.org/10.1038/s41467-023-39810-w
645 39. Lee, D. G., Kwon, E. Y., Kam, J., & Kug, J. S. (2025). Irreversible phytoplankton community
646 shifts over Subpolar North Atlantic in response to CO2 forcing. *Earth System Dynamics*, *16*(6),
647 2101-2111. https://doi.org/10.5194/esd-16-2101-2025
648 40. Stramma, L., Prince, E. D., Schmidtko, S., Luo, J., Hoolihan, J. P., Visbeck, M., et al.(2012).
649 Expansion of oxygen minimum zones may reduce available habitat for tropical pelagic fishes.
650 *Nature Climate Change*, *2*(1), 33-37. https://doi.org/10.1038/nclimate1304
651 41. Lynch-Stieglitz, J. (2017). The Atlantic meridional overturning circulation and abrupt climate
652 change. *Annual review of marine science*, *9*(1), 83-104. **https://doi.org/10.1146/annurev-**
653 **marine-010816-060415**
654 42. Ng, H. C., Robinson, L. F., McManus, J. F., Mohamed, K. J., Jacobel, A. W., Ivanovic, R. F., et
655 al. (2018). Coherent deglacial changes in western Atlantic Ocean circulation. *Nature*
656 *communications*, *9*(1), 2947. https://doi.org/10.1038/s41467-018-05312-3
657 43. Wang, Y., Costa, K. M., Lu, W., Hines, S. K., & Nielsen, S. G. (2024). Global oceanic
658 oxygenation controlled by the Southern Ocean through the last deglaciation. *Science Advances*,
659 *10*(3), 1-9. doi: 10.1126/sciadv.adk2

660 44. Barragán-Montilla, S., Johnstone, H. J., Mulitza, S., Reyes Macaya, D. A., Hoogakker, B. A., &
661 Pälike, H. (2025). Enhanced ventilation of Eastern North Atlantic Oxygen Minimum Zone with
662 deglacial slowdown of Meridional Overturning. *Nature Communications*, *16*(1), 1-10.
663 https://doi.org/10.1038/s41467-025-61177-3
664 45. Nave, S., Labeyrie, L., Gherardi, J., Caillon, N., Cortijo, E., Kissel, C., & Abrantes, F. (2007).
665 Primary productivity response to Heinrich events in the North Atlantic Ocean and Norwegian
666 Sea. *Paleoceanography*, *22*(3), 1-18. doi: https://doi.org/10.1029/2006PA001335
667 46. Mariotti, V., Bopp, L., Tagliabue, A., Kageyama, M., & Swingedouw, D. (2012). Marine
668 productivity response to Heinrich events: a model-data comparison. *Climate of the Past*, *8*(5),
669 1581-1598. https://doi.org/10.5194/cp-8-1581-2012
670 47. Buizert, C., Adrian, B., Ahn, J., Albert, M., Alley, R. B., Baggenstos, D., et al.. (2015). Precise
671 interpolar phasing of abrupt climate change during the last ice age. *Nature*, *520*(7549), 661-665.
672 https://doi.org/10.1038/nature14401
673 48. Hertzberg, J. E., Lund, D. C., Schmittner, A., & Skrivanek, A. L. (2016). Evidence for a
674 biological pump driver of atmospheric CO2 rise during Heinrich Stadial 1. *Geophysical Research*
675 *Letters*, *43*(23), 12-242. https://doi.org/10.1002/2016GL070723
676 Parekh, P., Follows, M. J., & Boyle, E. (2004). Modeling the global ocean iron cycle. *Global*
677 *biogeochemical cycles*, *18*(1). https://doi.org/10.1029/2003GB002061
678 49. Winkelmann, R., Dennis, D., Donges, J. F., Loriani, S., Klose, A. K., Abrams, J. F., et al. (2025).
679 The Tipping Points Modelling Intercomparison Project (TIPMIP): Assessing tipping point risks in
680 the Earth system. *EGUsphere* [preprint]. https://doi.org/10.5194/egusphere-2025-1899

50. Jones, C., Bossert, I., Dennis, D. P., Jeffery, H., Jones, C. D., Koenigk, T., Loriani, S., Sanderson, B., Séférian, R., Wyser, K., Yang, S., Abe, M., Bathiany, S., Braconnot, P., Brovkin, V., Burger, F. A., Cadule, P., Castruccio, F. S., Danabasoglu, G., Dittus, A., Donges, J. F., Fröb, F., Frölicher, T., Georgievski, G., Guo, C., Hu, A., Lawrence, P., Lerner, P., Licón-Saláiz, J., Otto-Bliesner, B., Romanou, A., Shevliakova, E., Silvy, Y., Swingedouw, D., Tjiputra, J., Walton, J., Wiltshire, A., Winkelmann, R., Wood, R., Yokohata, T., and Ziehn, T. (in review). The TIPMIP Earth system model experiment protocol: phase 1, *EGUsphere* [preprint]. https://doi.org/10.5194/egusphere-2025-3604, 2025.

51. Meinshausen, M., Nicholls, Z. R., Lewis, J., Gidden, M. J., Vogel, E., Freund, M., et al. (2020). The shared socio-economic pathway (SSP) greenhouse gas concentrations and their extensions to 2500. *Geoscientific Model Development*, *13*(8), 3571-3605.

52. Eyring, V., Bony, S., Meehl, G. A., Senior, C. A., Stevens, B., Stouffer, R. J., & Taylor, K. E. (2016). Overview of the Coupled Model Intercomparison Project Phase 6 (CMIP6) experimental design and organization. *Geoscientific Model Development*, *9*(5), 1937-1958. https://doi.org/10.5194/gmd-9-1937-2016

53. Russell, G. L., Miller, J. R., & Rind, D. (1995). A coupled atmosphere-ocean model for transient climate change studies. *Atmosphere-ocean*, *33*(4), 683-730. https://doi.org/10.1038/s41561-021-00790-5

54. Kelley, M., Schmidt, G. A., Nazarenko, L. S., Bauer, S. E., Ruedy, R., Russell, G. L. (2020). GISS-E2. 1: Configurations and climatology. *Journal of Advances in Modeling Earth Systems*, *12*(8), e2019MS002025. https://doi.org/10.1029/2019MS002025

55. Prather, M. J. (1986). Numerical advection by conservation of second-order moments. *Journal of Geophysical Research: Atmospheres*, *91*(D6), 6671-6681. https://doi.org/10.1029/JD091iD06p06671

56. Large, W. G., McWilliams, J. C., & Doney, S. C. (1994). Oceanic vertical mixing: A review and a model with a nonlocal boundary layer parameterization. *Reviews of geophysics*, *32*(4), 363-403. https://doi.org/10.1029/94RG01872

57. Gent, P. R., Willebrand, J., McDougall, T. J., & McWilliams, J. C. (1995). Parameterizing eddy-induced tracer transports in ocean circulation models. *Journal of physical oceanography*, *25*(4), 463-474. https://doi.org/10.1175/1520-0485(1995)025<0463:PEITTI>2.0.CO;2

58. Marshall, J., Scott, J. R., Romanou, A., Kelley, M., & Leboissetier, A. (2017). The dependence of the ocean's MOC on mesoscale eddy diffusivities: A model study. *Ocean Modelling*, *111*, 1-8. https://doi.org/10.1016/j.ocemod.2017.01.001

59. Romanou, A., Marshall, J., Kelley, M., & Scott, J. (2017). Role of the ocean's AMOC in setting the uptake efficiency of transient tracers. *Geophysical research letters*, *44*(11), 5590-5598. https://doi.org/10.1002/2017GL072972

60. Zhang, J., Rothrock, D., & Steele, M. (2000). Recent changes in Arctic sea ice: The interplay between ice dynamics and thermodynamics. *Journal of Climate*, *13*(17), 3099-3114. https://doi.org/10.1175/1520-0442(2000)013<3099:RCIASI>2.0.CO;2

61. Bitz, C. M., & Lipscomb, W. H. (1999). An energy-conserving thermodynamic model of sea ice. *Journal of Geophysical Research: Oceans*, *104*(C7), 15669-15677. https://doi.org/10.1029/1999JC900100

62. Schmidt, G. A., Bitz, C. M., Mikolajewicz, U., & Tremblay, L. B. (2004). Ice–ocean boundary conditions for coupled models. *Ocean Modelling*, *7*(1-2), 59-74. https://doi.org/10.1016/S1463-5003(03)00030-1

63. Ito, G., Romanou, A., Kiang, N. Y., Faluvegi, G., Aleinov, I., Ruedy, R., et al. (2020). Global carbon cycle and climate feedbacks in the NASA GISS ModelE2. 1. *Journal of Advances in Modeling Earth Systems*, *12*(10), e2019MS002030. https://doi.org/10.1029/2019MS002030

64. Romanou, A., Lerner, P., Kiang, N. Y., Alienov, I., Kelley, M., Miller, R, Russell, G., Ruedy, R., Schmidt, G., Hakuba, M.,& Wang, Ou. (in review). The NASA-GISS ModelE2.1-CC2 ESM: development and simulations. *Geoscientific Model Development*, [preprint]. https://doi.org/10.5194/egusphere-2025-4839

65. Orr, J. C., Najjar, R. G., Aumont, O., Bopp, L., Bullister, J. L., Danabasoglu, G., et al. (2017). Biogeochemical protocols and diagnostics for the CMIP6 Ocean Model Intercomparison Project (OMIP). *Geoscientific Model Development*, *10*(6), 2169-2199. https://doi.org/10.5194/gmd-10-2169-2017

66. Gregg, W. W., & Conkright, M. E. (2002). Decadal changes in global ocean chlorophyll. *Geophysical Research Letters*, *29*(15), 20-1. https://doi.org/10.1029/2002GL014689

67. Cotrim da Cunha, L., Buitenhuis, E. T., Le Quéré, C., Giraud, X., & Ludwig, W. (2007). Potential impact of changes in river nutrient supply on global ocean biogeochemistry. *Global Biogeochemical Cycles*, *21*(4). https://doi.org/10.1029/2006GB002718

68. Tibshirani, R. (2011). Regression shrinkage and selection via the lasso: a retrospective. *Journal of the Royal Statistical Society Series B: Statistical Methodology*, *73*(3), 273-282. doi: 1369–7412/11/73273

69. Wilson, J. D., Andrews, O., Katavouta, A., de Melo Viríssimo, F., Death, R. M., Adloff, M., Chelsey A. Baker, C. A., Blackledge, B., Goldsworth, F. W., Kennedy-Asser, A. T., Liu, Q., Sieradzan, K. R., Vosper, E., & Ying, R. (2022). The biological carbon pump in CMIP6 models: 21st century trends and uncertainties. *Proceedings of the National Academy of Sciences*, *119*(29), 1-3. doi: https://doi.org/10.1073/pnas.2204369119

70. Kopp, R. E., Shwom, R. L., Wagner, G., & Yuan, J. (2016). Tipping elements and climate–economic shocks: Pathways toward integrated assessment. *Earth's Future*, *4*(8), 346-372. https://doi.org/10.1002/2016EF000362

71. Lerner, P. (2026). Data, anaylysis Scripts, and source code for Cascading Impacts of AMOC weakening and collapse on Marine Biogeochemistry (Version v1) [Data set]. Zenodo. https://doi.org/10.5281/zenodo.18883081

72. Takahashi, T., Olafsson, J., Goddard, J. G., Chipman, D. W., & Sutherland, S. C. (1993). Seasonal variation of CO2 and nutrients in the high-latitude surface oceans: A comparative study. *Global Biogeochemical Cycles*, *7*(4), 843-878. https://doi.org/10.1029/93GB02263

Extended Data Legends:

Extended Fig. 1: Same as Fig. 1a-d in the main text, but showing actual values of AMOC (a,b), atmospheric CO2 (c), global mean surface air temperature (d), the air-sea CO2 flux (e), net primary productivity (f), intermediate-layer oxygen concentration (g), and Carbon Storage (h)

Extended Fig. 2: Air-Sea CO2 flux anomalies compared to the late historical (1980-2014 climatology) in (a) The subpolar North Atlantic, (b) the subtropical North Atlantic, (c) the Subtropical South Atlantic, (d) the Southern Ocean North of the Polar Front, (e) the Subpolar North Pacific, (f) the Arabian Sea, and (g) the Arctic Ocean. Red and blue curves show collapsed and recovered ensemble means (shading is +/- 1σ), respectively. The faint vertical dashed line shows the timing of the onset of AMOC collapse, while the opaque vertical dashed line shows the timing of the response of the flux to AMOC collapse. (h-n), (o-u), and (v-ab) are the same as (a-g), except for net primary productivity, intermediate layer O2 concentration, and carbon storage, respectively.

Extended Fig. 3: Difference in maximum mixed layer depth between the mean of ensemble members where AMOC collapses and recovers, averaged between years 2350 and 2400. (b) Atlantic zonal average difference in salinity and (c) potential density between the mean of ensemble members where AMOC collapses and recovers, averaged between years 2350 and 2400. (d,e) as in (b,c), but for the Pacific zonal averages.

Extended Fig. 4: Schematics of the cascading effects of AMOC collapse on ocean biogeochemical properties in different regions. Timescales refer to lags in Fig. 3. Image credit: Fiona Martin.

Extended Fig. 5: Flux of Ocean Age tracer at 1100 m in the Arabian Sea. Positive indicates a flux of older water from beneath 1100 m upward. (b) Vertical velocity at 1100 m (Positive = downwelling). Reduced upwelling leads to a reduction in the transport of deeper, older waters above 1100 m.

Extended Fig. 6: The right magenta circles show the change in the air-sea pCO2 gradient between the collapsed and recovered ensemble members in the subtropical South Atlantic, averaged between 2350-2400. The triangles to the left show, respectively, the contributions of SST, SSS, DIC, and alkalinity to this change. Contributions are obtained using the sensitivity of seawater pCO2 to changes in each of these fields from ref[72].

Extended Fig. 7: Sea surface temperature (SST) anomalies compared to the late historical (1980-2014 climatology) in (a) The subpolar North Atlantic, (b) the subtropical North Atlantic, (c) the Subtropical South Atlantic, (d) the Southern Ocean North of the Polar Front, (e) the Subpolar North Pacific, (f) the Arabian Sea, and (g) the Arctic Ocean. Red and blue curves show collapsed and recovered ensemble means (shading is +/- 1σ), respectively. The faint vertical dashed line shows the timing of the onset of AMOC collapse, while the opaque vertical dashed line shows the timing of the response of the flux to AMOC collapse. (h-n) are the same as (a-g), except for Surface Air Temperature (SAT).

Extended Fig. 8: AMOC at 48°N and 26.5°N for all ensemble members. Ensemble members a, b, d, and e recover before the year 2200, while members e and h recoveries are delayed until 2400 and 2550, respectively. Members c, g, and i show a full collapse by year 2350, with no recovery exhibited. Members f and j also show AMOC collapse, but delayed until years 2450 and 2580, respectively.

Extended Fig. 9: Change in ocean biogeochemical properties between collapsed and recovered ensemble means predicted by the LASSO regression model vs. simulated by the model. Samples are obtained between the years 2124 and 2300 and smoothed using a 20-yr moving average filter before the LASSO regression is applied. The red line shows the 1:1 line. Panels show LASSO regression results for the air-sea CO2 flux in (a) the subtropical North Atlantic, (b) the subpolar North Atlantic, (c) the subtropical South Atlantic, (d) the Arctic; NPP in (e) the subtropical North Atlantic, (f) the subpolar North Atlantic, (g) the subtropical South Atlantic, (h) the subpolar North Atlantic, and (i) the Southern Ocean North of the Polar front; Intermediate layer oxygen concentration in (j) the subtropical North Atlantic, (k) the subpolar North Atlantic, (l) the Arabian Sea, and (m) the subpolar North Atlantic; carbon storage in (n) the subtropical North Atlantic, and (o) the Arctic.

Extended Fig. 10: Differences between ocean biogeochemical properties in the collapsed and recovered runs, averaged between years 2350 and 2400, and attribution of these differences to

various drivers. In each region, triangles on the left always show the ocean biogeochemical property differences, and triangles to the right show the attribution to the various drivers. Upward pointing triangles mean that the biogeochemical property changes under AMOC collapse (in the case of red triangles), or that the driver causes an increase in the property considered (all other colors). Uncertainties in parentheses are +/- 1 standard deviation. Panels are for the same variables and regions as in Extended Fig. 9.

Supplementary Files

This is a list of supplementary files associated with this preprint. Click to download.

- ExtendedFig1submit.jpg
- ExtendedFig5submit.jpg
- ExtendedFig8submit.jpg
- ExtendedFig2submit.jpg
- ExtendedFig6submit.jpg
- ExtendedFig9submit.jpg
- ExtendedFig3submit.jpg
- ExtendedFig10submit.jpg
- ExtendedFig7submit.jpg
- ExtendedFig4submit.jpg